ORIGINAL PAPER

Nagoya J. Med. Sci. **84**. 269–285, 2022
doi:10.18999/nagjms.84.2.269

Radiomics analysis for differentiating of cervical lymphadenopathy between cancer of unknown primary and malignant lymphoma on unenhanced computed tomography

Hayato Tomita[1,2], Tsuneo Yamashiro[1], Gyo Iida[1], Maho Tsubakimoto[1], Hidefumi Mimura[2] and Sadayuki Murayama[1]

[1]*Department of Radiology, University of the Ryukyus Graduate School of Medicine, Nishihara, Japan*
[2]*Department of Radiology, St. Marianna University School of Medicine, Kawasaki, Japan*

ABSTRACT

To investigate the usefulness of texture analysis to discriminate between cervical lymph node (LN) metastasis from cancer of unknown primary (CUP) and cervical LN involvement of malignant lymphoma (ML) on unenhanced computed tomography (CT). Cervical LN metastases in 17 patients with CUP and cervical LN involvement in 17 patients with ML were assessed by ^{18}F-FDG PET/CT. The texture features were obtained in the total cross-sectional area (CSA) of the targeted LN, following the contour of the largest cervical LN on unenhanced CT. Values for the max standardized uptake value (SUVmax) and the mean SUV value (SUVmean), and 34 texture features were compared using a Mann-Whitney U test. The diagnostic accuracy and area under the curve (AUC) of the combination of the texture features were evaluated by support vector machine (SVM) with nested cross-validation. The SUVmax and SUVmean did not differ significantly between cervical LN metastases from CUP and cervical LN involvement from ML. However, significant differences of 9 texture features of the total CSA were observed (p = 0.001 – 0.05). The best AUC value of 0.851 for the texture feature of the total CSA were obtained from the correlation in the gray-level co-occurrence matrix features. SVM had the best AUC and diagnostic accuracy of 0.930 and 84.8%. Radiomics analysis appears to be useful for differentiating cervical LN metastasis from CUP and cervical LN involvement of ML on unenhanced CT.

Keywords: texture, cancer of unknown primary, malignant lymphoma, cervical lymphadenopathy, machine learning

Abbreviations:
LN: cervical lymph node
CUP: cancer of unknown primary
ML: malignant lymphoma
CT: computed tomography
^{18}F-FDG PET: fluorine-18-2-fluoro-2-deoxy-D-glucose positron emission tomography
SUV: standardized uptake value
VOI: volume of interest
ROI: region of interest

Received: April 26, 2021; accepted: August 3, 2021

Corresponding Author: Hayato Tomita, MD, PhD
Department of Radiology, University of the Ryukyus Graduate School of Medical Science, 207 Uehara, Nishihara-cho, Nakagami-gun 903-0215, Japan
Tel: +81-98-895-1162, E-mail: hayato.tomita@marianna-u.ac.jp

CSA: cross-sectional area
AUC: area under the curve
SVM: support vector machine
RFE: recursive feature elimination
GLCM: gray-level co-occurrence matrix features
GLRLM: gray-level run-length matrix features
NGLDM: neighborhood gray-level different matrix
GLZLM: gray-level zone length matrix

INTRODUCTION

Enlarged cervical lymph nodes (LNs) have been reported to indicate malignancy in over 50% of cases.[1,2] Cervical LN metastasis from head and neck carcinoma and cervical LN involvement of malignant lymphoma (ML) in the head and neck are the most common disease associated with cervical LN malignancy.[2,3] Cancer of unknown primary (CUP) is defined as metastatic disease without evidence of a primary tumor on physical examination, endoscopy, or imaging. Cervical LN metastasis from CUP accounts for up to 7% of all head and neck carcinomas.[4,5] Discrimination between cervical LN metastasis from CUP and cervical LN involvement of ML is challenging when the primary cancer in the head and neck is not detected on initial evaluation. Fine-needle aspiration/biopsy are performed to confirm tissue characteristics of cervical lymphadenopathy in cases of suspected malignancy. Diagnosis of ML requires sufficient tissue for histological, immunophenotypic, and genetic studies to identify the ML subtype and determine the optimal treatment strategy.[6,7] In addition, patients with cervical LN enlargement might undergo random biopsy of the larynx and pharynx to identify the primary tumor site. Unfortunately, such invasive approaches are associated with a risk of complications and a possibility of insufficient materials.[6-9]

Computed tomography (CT) is performed to evaluate the presence of inflammation and metastasis, primary malignant tumor location, degree of extracapsular extension, and ML stage when cervical lymphadenopathy is identified clinically. The imaging findings for cervical LN metastasis from CUP and cervical LN involvement of ML on CT and magnetic resonance can be similar.[10] Therefore, differentiating between cervical LN metastasis from CUP and cervical LN involvement of ML is currently challenging. Recently, artificial intelligence has been applied to medical imagings.[11-17] Also, quantitative imaging analysis has been developed to improve diagnostic performance with increasing reproducibility and decreasing variability between radiologists. Texture analysis, a mathematical method used to calculate differences in gray-level patterns, has the potential to evaluate tumor characteristics, predict response to therapy, and determine prognosis in patients with malignant tumors.[18-25] However, no previous studies have described the differentiation between cervical LN metastasis from CUP and cervical LN involvement of ML using texture analysis. Therefore, we hypothesized that CT-based texture features using machine learning can discriminate between cervical LN metastasis from CUP and cervical LN involvement of ML. The aim of this study is to investigate the diagnostic accuracy of texture analysis in differentiating cervical LN metastasis from CUP and cervical LN involvement of ML on unenhanced CT.

MATERIALS AND METHODS

This retrospective study was approved by our institutional review board, which waived the need for informed consent from patients.

Subjects

Initially, 57 patients with histopathologically proven cervical LN metastasis from CUP (n=17) and ML (n=40) who underwent fluorine-18-2-fluoro-2-deoxy-D-glucose positron emission tomography (^{18}F-FDG PET)/CT from April 2013 to April 2018 were identified.

Inclusion criteria for CUP with cervical LN metastasis

All patients with cervical LN metastases from CUP fulfilled the following inclusion criteria: 1) a physical examination and nasal endoscopy by a otolaryngologist and an ^{18}F-FDG PET/CT before treatment were performed and failed to identify the original cancer site; 2) metastases of enlarged cervical LN(s) were proven histopathologically by neck dissection or fine-needle biopsy; and 3) the treatment for CUP was ultimately performed based on the diagnosis of cervical LN metastasis from CUP, and on a discussion by otolaryngologists and radiologists. Because some patients were treated prior to implementation of the recommendation to evaluate Epstein-Barr virus (EBV) and human papilloma virus (HPV) infection status for occult cervical cancer,[26] it was not necessary to evaluate EBV or HPV infection status for all patients.

Inclusion criteria for cervical LN involvement of ML

Seventeen patients were enrolled in this study based on the following criteria: 1) abnormal FDG uptake was visually identified in the enlarged cervical LN on ^{18}F-FDG PET/CT and 2) ML was confirmed by fine-needle biopsy of the enlarged neck LNs.

FDG-PET/CT scanning

All patients who had fasted for at least 5 hours underwent whole-body ^{18}F-FDG-PET/CT (the Biograph mCT-S(64)4R; Siemens Healthineers, Forchheim, Germany) from the vertex of the skull to the floor of the pelvis. ^{18}F-FDG (3.7 MBq/kg BW, max 340MBq) was given intravenously. CT was performed 1 hour after ^{18}F-FDG injection. The following scan parameters for the 64-row whole-body PET/CT scanner were used: tube voltage, 120 kVp; tube current, automatic exposure control (CARE Dose 4D); gantry rotation time, 0.5 sec; beam pitch, 1.5; imaging field of view, 500 × 500 mm; matrix, 512 × 512; and slice thickness, 2mm. All images were reconstructed with a B31f kernel. PET data were reconstructed using a three-dimensional (3D) iterative algorithm of ordered subsets expectation-maximization (OSEM) (2 iterations, 21 subsets).

^{18}F-FDG PET image analysis

All PET data were reviewed on a commercially available workstation (Syngo via VB10; Siemens Healthineers). The boundary of volume of interest (VOI) for PET was semi-automatically drawn by the workstation in the largest enlarged cervical LN. The maximum standardized uptake value (SUVmax: SUV of the highest count within the VOI) and the mean SUV value (SUVmean: SUV of the mean count within the VOI) were calculated automatically by the workstation.

Image segmentation and texture analysis

On the axial planes of the CT images, the texture features were analyzed in the total cross-sectional area (CSA) of the target lesion. On each axial CT image, the regions of interest (ROIs) were placed to include the targeted LN. LNs were manually countered by consensus of

two radiologists (**blinded** and **blinded**, who had 7 and 19 years of experience in radiology, respectively) using LifeX Software (https://www.lifexsoft.com, CEA, Saclay, France).[27] CT images with severe metal artifacts were not analyzed. Texture features were classified as follows: 4 histogram features, 6 gray-level co-occurrence matrix (GLCM) features, 11 gray-level run length matrix (GLRLM) features, 2 neighborhood gray-level different matrix (NGLDM) features, and 11 gray-level zone length matrix (GLZLM) features. A list of all texture features is provided in Appendix 1.

Statistical analysis

JMP 10.0.2 software (SAS Institute, Cary, NC, USA) was used for statistical analyses. Data were expressed as the mean ± standard deviation. A Mann-Whitney test was used to compare the SUVmax, SUVmean, and 34 texture features of the total CSA between the cervical LN metastases from CUP and the cervical LN involvement from ML. Receiver operating characteristic (ROC) curves and the area under the curve (AUC) of the ROC were calculated for each texture feature. A python-based support vector machine (SVM) with radial basis kernel in the machine learning library 'scikit-learn' (v0.16.1; http://scikit-learn.org) was implemented to evaluate accuracy and AUC for combinations of texture features with a nested cross-validation (10 repetition of 5-fold inner cross-validation and 10 repetition of 5-fold outer cross-validation) (Fig 1). A non-nested cross-validation has a bias that refers to the same data to optimize model parameters and evaluate model performances.[28] In a nested cross-validation, different data between tuning parameters and evaluating model performances are used to avoid overfitting: 1) an outer 5-fold cross-validation splits all data into 4 training sets and 1 test set; 2) an inner 5-fold cross-validation splits the training data into another 4 training set and 1 test set; 3) parameters are tuned in an inner 5-fold cross-validation that is repeated 10 times; 4) a remaining test set in an outer 5-fold cross-validation is used to evaluate SVM performance using the optimized parameters; and 5) the series of processes are performed in an outer 5-fold cross-validation, which is repeated 10 times.[29,30] The grid search method was used to select the optimized SVM parameters: C and gamma. The best combinations of the texture features were selected by a cursive feature

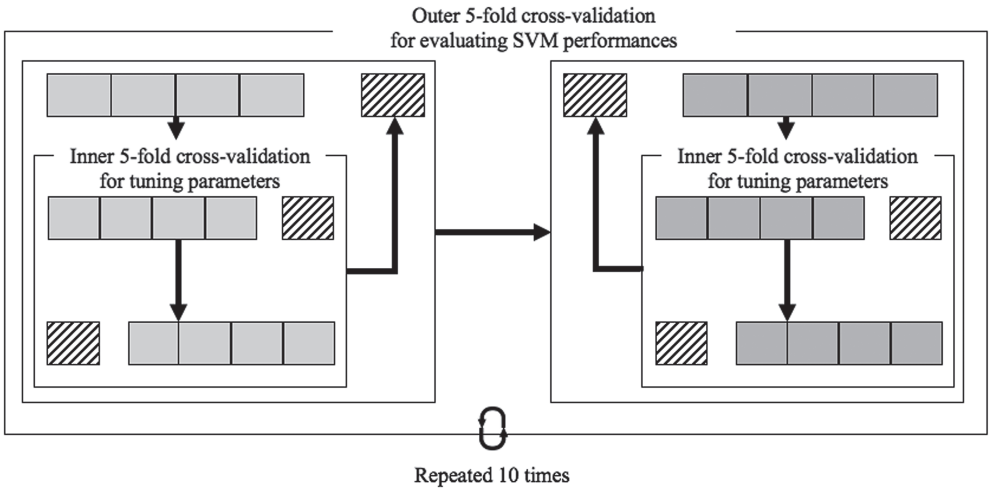

Fig. 1 Machine learning using nested cross-validation

elimination (RFE) method. RFE reduced the combination of texture features to specified number of top texture features according to importance.[31] All *p*-values less than 0.05 were considered to indicate significant difference.

RESULTS

A total of 34 patients were included. Pretreatment characteristics of patients and tumors are shown in Table 1. Measurements of CT-related radiation dose were calculated by CT dose index (CTDI). The mean CTDIvol was 4.73±3.41 mGy.

Table 1 Characteristics of patients and tumors

	CUP		ML	
Age mean±SD	65.9±3.5		64.6±14.4	
Gender male/female	14/3		10/7	
Histological types	Pooly differenciated SCC	8	Diffuse large B-cell lymphoma	14
	Moderate differenciated SCC	1	Adult T-cell lymphoma	2
	Nonkeratinizing differenciated SCC	1	angioimmunoblastic T-cell lymphoma	1
	Sarcomatoid SCC	1		
	SCC;Undefined	6		
Clinical stage			I	0
			II	3
			III	1
			IV	13

SD: standard deviation
CUP: cancer of unknown primary
ML: malignant lymphoma
SCC: squamous cell carcinoma

Comparisons of SUVmax and SUVmean between cervical LN metastasis from CUP and cervical LN involvement of ML

Table 2 shows the SUVmax and SUVmean measurements. The differences in SUVmax and SUVmean between cervical LN metastasis from CUP and cervical LN involvement of ML were not statistically significant.

Table 2 Comparisons of SUVmax and SUVmean between cervical LN metastasis from CUP and cervical LN involvement of ML

	Cervical LN metastasis from CUP		**Cervical LN involvement from ML**		
	Mean	SD	Mean	SD	*p*
SUVmax	16.01	4.42	17.06	9.43	0.718
SUVmean	9.72	3.19	10.43	5.84	0.877

LN: lymph node
SUV: standardized uptake value
CUP: cancer of unknown primary
ML: malignant lymphoma
SD: standard deviation

Comparisons of texture features between cervical LN metastasis from CUP and cervical LN involvement of ML

Measurements of 34 texture features and correlations between tumor voxel and texture features are shown in Appendix 2 and 3, respectively. Texture features that had a strong correlation coefficient of >0.7 between tumor voxel were excluded to avoid influence of the confounding factor.[32]

Table 3 summarize the p-value, sensitivity, specificity, accuracy, and AUC of the selected texture features. Significant differences in 9 texture features in the total CSA that discriminated cervical LN metastases from CUP and cervical LN involvement from ML were observed. The highest AUC in the total CSA, which were obtained from the correlation in GLCM, were 0.851, respectively.

The highest AUC and accuracy by SVM were 0.930 and 84.8%, respectively, with a combination of the kurtosis in Histogram, the correlation in GLCM, and the coarseness in the NGLDM as shown in Table 4 and Fig 2. Fig 3 show representative cases in which differences between cervical LN metastasis from CUP and cervical LN involvement of ML were identified using the combination of texture features.

Table 3 AUC for selected texture features in the maximum cross-sectional area to discriminate between cervical LN metastasis from CUP and cervical LN involvement of ML

	Cervical LN metastasis from CUP		**Cervical LN involvement of ML**							
	Mean	SD	Mean	SD	*p*	cut-off	SEN (%)	SPE (%)	ACC (%)	AUC
Histogram										
Kurtosis	3.634	0.588	3.108	0.251	0.006*	3.24	82.4	76.5	79.4	0.844
Entropy	0.851	0.069	0.782	0.092	0.012*	0.82	70.6	70.6	70.6	0.753
Energy	0.169	0.029	0.195	0.041	0.020*	0.18	64.7	70.6	67.6	0.732
GLCM										
Energy	0.031	0.012	0.042	0.019	0.025*	0.043	52.9	94.1	73.5	0.725
Correlation	0.193	0.074	0.092	0.058	0.001*	0.105	76.5	94.1	85.3	0.851
Entropy	1.673	0.142	1.538	0.185	0.019*	1.500	47.1	94.1	70.6	0.734

NGLDM										
Coarseness	0.002	0.005	0.009	0.012	0.001*	0.004	62.7	88.2	79.4	0.830
GLZLM										
SZE	0.686	0.019	0.635	0.083	0.048*	0.665	58.8	82.3	73.5	0.689
HGZE	10874	119	10966	117	0.037*	11030	35.3	100	67.6	0.709

CUP: cancer of unknown primary
ML: malignant lymphoma
SD: standard deviation
SEN: sensitivity
SPE: specificity
ACC: accuracy
AUC: the area under the curve
GLCM: gray-level co-occurrence matrix
NGLDM: neighborhood gray-level different matrix
GLZLM: gray-level zone length matrix
SZE: short-zone emphasis
HGRE: high gray-level run emphasis
* indicates significant differences.

Table 4 The best AUC for the combination of texture features using SVM

	SEN (%)	SPE (%)	ACC (%)	AUC
Kurtosis in Histogram, Correlation in GLCM, and Coarseness in NGLDM	82.6	98.9	84.8	0.930

SEN: sensitivity
SPE: specificity
ACC: accuracy
AUC: the area under the curve
SVM: support vector machine
GLCM: gray-level co-occurrence matrix features
NGLDM: neighborhood gray-level different matrix

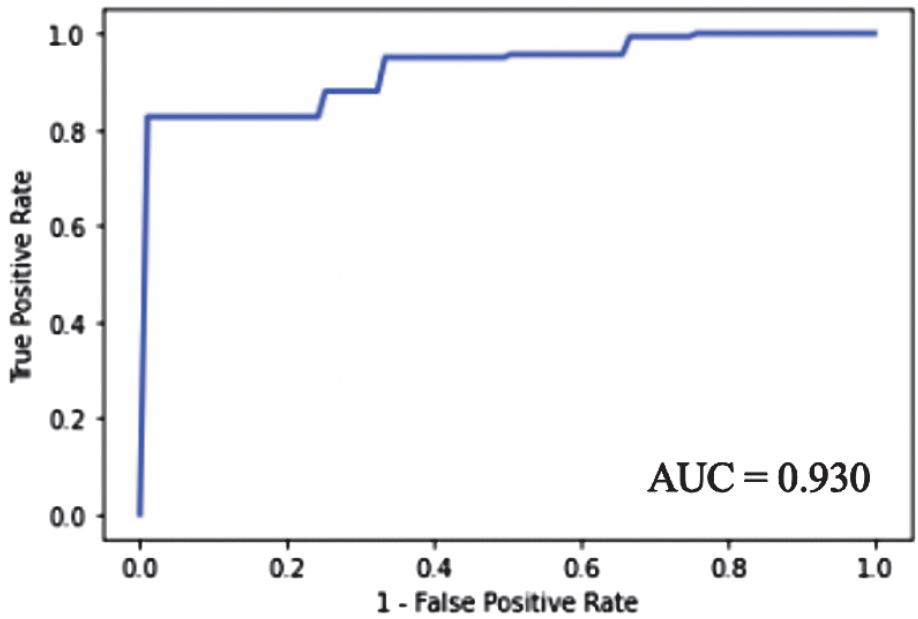

Fig. 2 The ROC curves of the best combination of selected texture features

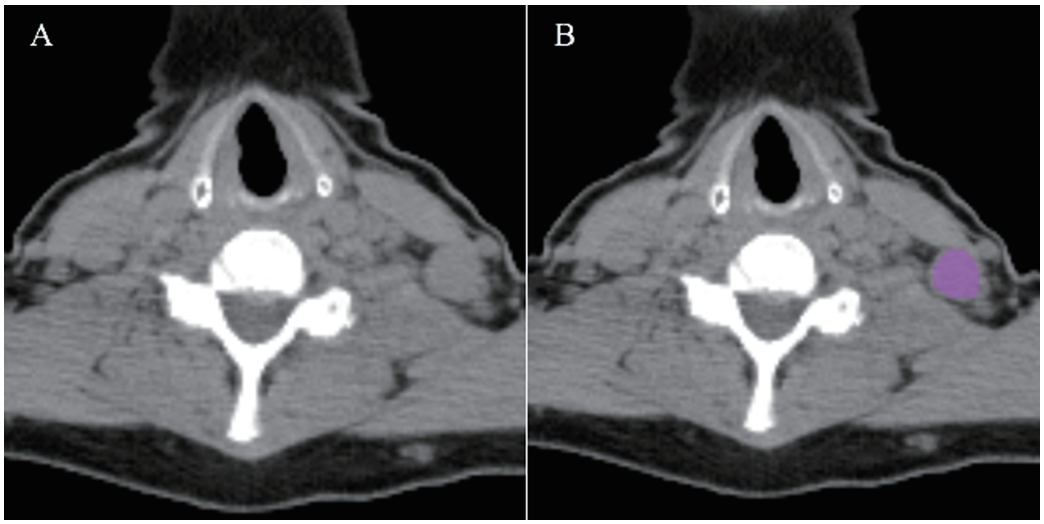

Fig. 3 A 70-year-old female with cervical LN involvement from ML
The correlation in the GLCM (0.018; cut-off values <0.110), the coarseness in the NGLDM (0.036; cut-off values >0.002), the kurtosis in the histogram (2.490; cut-off values <3.290), all derived from the total cross-sectional area, revealed true positives, while the SUVmax and SUVmean values were 9.88 and 6.02, respectively (A and B).
GLCM: gray-level co-occurrence matrix features
NGLDM: neighborhood gray-level different matrix
SZE: short-zone emphasis
GLZLM: gray-level zone length matrix

DISCUSSION

This study demonstrates that 9 texture features of the total CSA of the enlarged cervical LNs on unenhanced CT, differentiated cervical LN metastases with CUP versus cervical LN involvement from ML; however, no significant differences in the SUVmax or SUVmean were observed. Thus, it can be considered that radiomics analysis might provide useful information for the differentiation of cervical lymphadenopathy between CUP and ML.

Head-and-neck CT for cervical lymphadenopathy has been performed to evaluate the location, abnormal internal architecture, extra-nodal metastasis, and primary site of malignant tumors. Notably, the necrotic components that have a key role in the evaluation of malignancy are frequently estimated by the enhancement pattern on a head-and-neck CT with contrast media.[33,34] On unenhanced CT, it is difficult to detect small changes in CT attenuation objectively; such changes are likely to be diagnosed based on radiologists' impression. Several previous studies have demonstrated that texture analysis can be used to evaluate correlations between imaging findings on unenhanced CT and pathological findings and to differentiate between malignant and benign tumors.[35-37] Cell proliferation, myxoid changes, abnormal angiogenesis, and necrotic changes within malignant tumors result in heterogeneity.[37] Central necrosis in cervical LNs that reflects reduced CT attenuation is recognized as indicating metastasis.[36,39] Furthermore, ML appears as isoattenuation in a homogenous mass.[39] Nodal lymphoma is characterized by high cellularity, large nuclei, and less extracellular space than well or moderate differentiated carcinomas.[34,41] In the present study, unenhanced CT-based quantitative analysis of texture features could be used to differentiate between cervical LN metastases from CUP and cervical LN involvement from ML. Texture features related to randomness, such as entropy in the GLCM, in cases with cervical LN metastases from CUP were higher than those with cervical LN involvement from ML and the coarseness in the NGLDM related to homogeneity was lower. Some texture features could depict the gray-level differences between cervical LN metastasis from CUP and cervical LN involvement of ML on unenhanced CT.

Unenhanced CT was performed with a low radiation dose in the current study. Reduced radiation doses lead to decreased image quality due to a decrease in photons. However, unenhanced low-dose CT might be useful for quantifying enlarged cervical LN. A previous study reported that CT-based texture analysis is not affected by changes in tube current on CT in a phantom study; thus, findings support the present results.[42]

This study has some limitations. First, we had a small number of patients in this retrospective and single institutional study. Second, occult EBV-related nasopharyngeal cancers and occult HPV-related oropharyngeal cancers were not excluded due to the inclusion of patients who were treated before the recommendation to evaluate EBV and HPV infection status was implemented. Third, the ROIs for the cervical LNs were manually delineated. Fourth, the degree of aggressiveness of each ML was not evaluated. Ganshan et al suggested the possibility that CT-based texture analysis for ML may be correlated with fibrosis, which appears in a variety of patterns in ML subtypes.[42] Necrosis within adult T-cell lymphoma lesions has previously been described to be correlated with poor prognosis.[43] The aggressiveness of ML can affect texture analysis. Therefore, further large-scale studies that evaluate more parameters and classify ML based on the degree of aggressiveness are required.

In conclusion, CT-based texture analysis can distinguish cervical LN metastasis from CUP and enlarged cervical LNs in ML, while the SUVmax and SUVmean cannot differentiate them. Quantitative analysis of texture features on unenhanced CT has the potential to provide additional information about patients with malignant cervical lymphadenopathy.

CONFLICT OF INTEREST

The authors have declared no conflicts of interest.

REFERENCES

1 Roland N, Bradley PJ. Neck swellings. *BMJ*. 2014;348:g1078. doi:10.1136/bmj.g1078.
2 Yang L, Luo D, Li L, et al. Differentiation of malignant cervical lymphadenopathy by dual-energy CT: A preliminary analysis. *Sci Rep*. 2016;6:31020. doi:10.1038/srep31020.
3 Kato H, Kanematsu M, Watanabe H, Kawaguchi S, Mizuta K, Aoki M. Differentiation of extranodal non-hodgkins lymphoma from squamous cell carcinoma of the maxillary sinus: A multimodality imaging approach. *Springerplus*. 2015;4:228. doi:10.1186/s40064-015-0974-y.
4 Müller von der Grün J, Tahtali A, Ghanaati S, Rödel C, Balermpas P. Diagnostic and treatment modalities for patients with cervical lymph node metastases of unknown primary site - current status and challenges. *Radiat Oncol*. 2017;12(1):82. doi:10.1186/s13014-017-0817-9.
5 Miller FR, Karnad AB, Eng T, Hussey DH, Stan McGuff H, Otto RA. Management of the unknown primary carcinoma: Long-term follow-up on a negative PET scan and negative panendoscopy. *Head Neck*. 2008;30(1):28–34. doi:10.1002/hed.20654.
6 Cheson BD, Fisher RI, Barrington SF, et al. Recommendations for initial evaluation, staging, and response assessment of hodgkin and non-hodgkin lymphoma: The lugano classification. *J Clin Oncol*. 2014;32(27):3059–3068. doi:10.1200/JCO.2013.54.8800.
7 Pugliese N, Di Perna M, Cozzolino I, et al. Randomized comparison of power doppler ultrasonography-guided core-needle biopsy with open surgical biopsy for the characterization of lymphadenopathies in patients with suspected lymphoma. *Ann Hematol*. 2017;96(4):627–637. doi:10.1007/s00277-017-2926-9.
8 Zhuang SM, Wu XF, Li JJ, Zhang GH. Management of lymph node metastases from an unknown primary site to the head and neck (review). Mol Clin Oncol. 2014;2(6):917–922. doi:10.3892/mco.2014.361.
9 He Y, Ji X, Xie Y, et al. Clinical application of ultrasound-guided core needle biopsy with multiple punches in the diagnosis of lymphoma. *World J Surg Oncol*. 2015;13:126. doi:10.1186/s12957-015-0537-2.
10 King AD, Lei KI, Ahuja AT. MRI of neck nodes in non-hodgkin's lymphoma of the head and neck. *Br J Radiol*. 2004;77(914):111–115. doi:10.1259/bjr/53555208.
11 Kuno H, Qureshi MM, Chapman MN, et al. CT texture analysis potentially predicts local failure in head and neck squamous cell carcinoma treated with chemoradiotherapy. *AJNR Am J Neuroradiol*. 2017;38(12):2334–2340. doi:10.3174/ajnr.A5407.
12 Zhang H, Graham CM, Elci O, et al. Locally advanced squamous cell carcinoma of the head and neck: CT texture and histogram analysis allow independent prediction of overall survival in patients treated with induction chemotherapy. *Radiology*. 2013;269(3):801–809. doi:10.1148/radiol.13130110.
13 Koda E, Yamashiro T, Onoe R, et al. CT texture analysis of mediastinal lymphadenopathy: Combining with US-based elastographic parameter and discrimination between sarcoidosis and lymph node metastasis from small cell lung cancer. *PLoS One*. 2020;15(12):e0243181. doi:10.1371/journal.pone.0243181.
14 Ariji Y, Sugita Y, Nagao T, et al. CT evaluation of extranodal extension of cervical lymph node metastases in patients with oral squamous cell carcinoma using deep learning classification. *Oral Radiol*. 2020;36(2):148–155.doi:10.1007/s11282-019-00391-4.
15 Yanagawa M, Niioka H, Hata A, et al. Application of deep learning (3-dimensional convolutional neural network) for the prediction of pathological invasiveness in lung adenocarcinoma: A preliminary study. *Medicine (Baltimore)*. 2019;98(25):e16119. doi:10.1097/MD.0000000000016119.
16 Zhao X, Xie P, Wang M, et al. Deep learning-based fully automated detection and segmentation of lymph nodes on multiparametric-mri for rectal cancer: A multicentre study. *EBioMedicine*. 2020;56:102780. doi:10.1016/j.ebiom.2020.102780.
17 Tomita H, Yamashiro T, Heianna J, et al. Deep learning for the preoperative diagnosis of metastatic cervical lymph nodes on contrast-enhanced computed ToMography in patients with oral squamous cell carcinoma. *Cancers (Basel)*. 2021;13(4):600. doi:10.3390/cancers13040600.
18 Buch K, Fujita A, Li B, Kawashima Y, Qureshi MM, Sakai O. Using texture analysis to determine human papillomavirus status of oropharyngeal squamous cell carcinomas on CT. *AJNR Am J Neuroradiol*. 2015;36(7):1343–1348. doi:10.3174/ajnr.A4285.
19 Schieda N, Thornhill RE, Al-Subhi M, et al. Diagnosis of sarcomatoid renal cell carcinoma with CT: Evaluation by qualitative imaging features and texture analysis. *AJR Am J Roentgenol*. 2015;204(5):1013–1023.

doi:10.2214/AJR.14.13279.
20 Kirienko M, Cozzi L, Antunovic L, et al. Prediction of disease-free survival by the PET/CT radiomic signature in non-small cell lung cancer patients undergoing surgery. *Eur J Nucl Med Mol Imaging*. 2018;45(2):207–217. doi:10.1007/s00259-017-3837-7.
21 Tomita H, Kuno H, Sekiya K, et al. Quantitative assessment of thyroid nodules using dual-energy computed tomography: Iodine concentration measurement and multiparametric texture analysis for differentiating between malignant and benign lesions. *Int J Endocrinol*. 2020;2020:5484671. doi:10.1155/2020/5484671.
22 Tomita H, Yamashiro T, Heianna J, et al. Nodal-based radiomics analysis for identifying cervical lymph node metastasis at levels I and II in patients with oral squamous cell carcinoma using contrast-enhanced computed tomography. *Eur Radiol*. 2021;31(10):7440–7449. doi:10.1007/s00330-021-07758-4.
23 Tomita H, Yamashiro T, Iida G, Tsubakimoto M, Mimura H, Murayama S. Unenhanced CT texture analysis with machine learning for differentiating between nasopharyngeal cancer and nasopharyngeal malignant lymphoma. *Nagoya J Med Sci*. 2021;83(1):135–149. doi:10.18999/nagjms.83.1.135.
24 Tomori Y, Yamashiro T, Tomita H, et al. CT radiomics analysis of lung cancers: Differentiation of squamous cell carcinoma from adenocarcinoma, a correlative study with FDG uptake. *Eur J Radiol*. 2020;128:109032. doi:10.1016/j.ejrad.2020.109032.
25 Ridge J, Lydiatt W, Patel S, et al. *AJCC cancer staging manual*. 8th ed. New York: Springer;2017:79–94.
26 Nioche C, Orlhac F, Boughdad S, et al. LIFEx: A freeware for radiomic feature calculation in multimodality imaging to accelerate advances in the characterization of tumor heterogeneity. *Cancer Res*. 2018;78(16):4786–4789. doi:10.1158/0008-5472.CAN-18-0125.
27 Mwangi B, Tian TS, Soares JC. A review of feature reduction techniques in neuroimaging. *Neuroinformatics*. 2014;12(2):229–244. doi:10.1007/s12021-013-9204-3.
28 Bektas CT, Kocak B, Yardimci AH, et al. Clear cell renal cell carcinoma: Machine learning-based quantitative computed tomography texture analysis for prediction of fuhrman nuclear grade. *Eur Radiol*. 2019;29(3):1153–1163. doi:10.1007/s00330-018-5698-2.
29 Suh HB, Choi YS, Bae S, et al. Primary central nervous system lymphoma and atypical glioblastoma: Differentiation using radiomics approach. *Eur Radiol*. 2018;28(9):3832–3839. doi:10.1007/s00330-018-5368-4.
30 Feng Z, Rong P, Cao P, et al. Machine learning-based quantitative texture analysis of CT images of small renal masses: Differentiation of angiomyolipoma without visible fat from renal cell carcinoma. *Eur Radiol*. 2018;28(4):1625–1633. doi:10.1007/s00330-017-5118-z.
31 Mukaka MM. Statistics corner: A guide to appropriate use of correlation coefficient in medical research. *Malawi Med J*. 2012;24(3):69–71.
32 King AD, Tse GM, Ahuja AT, et al. Necrosis in metastatic neck nodes: Diagnostic accuracy of CT, MR imaging, and US. *Radiology*. 2004;230(3):720–726. doi:10.1148/radiol.2303030157.
33 Abdel Razek AA, Soliman NY, Elkhamary S, Alsharaway MK, Tawfik A. Role of diffusion-weighted MR imaging in cervical lymphadenopathy. *Eur Radiol*. 2006;16(7):1468–1477. doi:10.1007/s00330-005-0133-x.
34 Hodgdon T, McInnes MD, Schieda N, Flood TA, Lamb L, Thornhill RE. Can quantitative CT texture analysis be used to differentiate fat-poor renal angiomyolipoma from renal cell carcinoma on unenhanced CT images? *Radiology*. 2015;276(3):787–796. doi:10.1148/radiol.2015142215.
35 Ganeshan B, Goh V, Mandeville HC, Ng QS, Hoskin PJ, Miles KA. Non-small cell lung cancer: Histopathologic correlates for texture parameters at CT. *Radiology*. 2013;266(1):326–336. doi:10.1148/radiol.12112428.
36 Liu S, Zheng H, Pan X, et al. Texture analysis of CT imaging for assessment of esophageal squamous cancer aggressiveness. *J Thorac Dis*. 2017;9(11):4724–4732. doi:10.21037/jtd.2017.06.46.
37 Bayanati H, E Thornhill R, Souza CA, et al. Quantitative CT texture and shape analysis: Can it differentiate benign and malignant mediastinal lymph nodes in patients with primary lung cancer? *Eur Radiol*. 2015;25(2):480–487. doi:10.1007/s00330-014-3420-6.
38 Kato H, Kanematsu M, Watanabe H, Kawaguchi S, Mizuta K, Aoki M. Differentiation of extranodal non-hodgkins lymphoma from squamous cell carcinoma of the maxillary sinus: A multimodality imaging approach. *Springerplus*. 2015;4:228. doi:10.1186/s40064-015-0974-y.
39 Toma P, Granata C, Rossi A, Garaventa A. Multimodality imaging of hodgkin disease and non-hodgkin lymphomas in children. *Radiographics*. 2007;27(5):1335–1354. doi:10.1148/rg.275065157.
40 Holzapfel K, Duetsch S, Fauser C, Eiber M, Rummeny EJ, Gaa J. Value of diffusion-weighted MR imaging in the differentiation between benign and malignant cervical lymph nodes. *Eur J Radiol*. 2009;72(3):381–387. doi:10.1016/j.ejrad.2008.09.034.
41 Buch K, Li B, Qureshi MM, Kuno H, Anderson SW, Sakai O. Quantitative assessment of variation in CT parameters on texture features: Pilot study using a nonanatomic phantom. *AJNR Am J Neuroradiol*. 2017;38(5):981–985. doi:10.3174/ajnr.A5139.

42 Ganeshan B, Miles KA, Babikir S, et al., CT-based texture analysis potentially provides prognostic information complementary to interim fdg-pet for patients with hodgkin's and aggressive non-hodgkin's lymphomas. *Eur Radiol*. 2017;27(3):1012–1020. doi:10.1007/s00330-016-4470-8.

43 Bittencourt AL, Barbosa HS, Vieira MD, Farré L, Adult T-cell leukemia/lymphoma (ATL) presenting in the skin: clinical, histological and immunohistochemical features of 52 cases. *Acta Oncol*. 2009;48(4):598–604. doi:10.1080/02841860802657235.

Appendixes

Appendix 1

1. Histogram features

Histogram features consist of simple statistics that are associated with pixel values in images while spatial patterns of pixel values are not included. Skewness, kurtosis, entropy, and energy were calculated.

2. Gray-level co-occurrence matrix (GLCM) features

GLCM is defined as the distribution of co-occurring pixel values that are calculated from 4 directions in 2-dimentional space (2D) or 13 directions in 3-dimentional space (3D):

Homogeneity = $\sum_{i,j} \frac{p(i,j)}{1+|i-j|}$

Energy = $\sum_{i,j} p(i,j)^2$

Contrast = $\sum_{i,j} |i-j|^2 p(i,j)$

Correlation = $\sum_{i,j} \frac{(i-\mu_i)(j-\mu_j)p(i,j)}{\sigma_i \sigma_j}$

Entropy = $\sum_{i,j} \log(p(i,j))p(i,j)$

Dissimilarity = $\sum_{i,j} |i-j|p(i,j)$

Where p(*i,j*) represents (*i,j*) value of the GLCM.

3. Gray-level run-length matrix (GLRLM) features

The GLRLM means the number of the consecutive pixels of the same gray-level value for 4 directions in 2D or 13 directions in 3D:

Short run emphasis (SRE) = $\frac{1}{n_r} \sum_{i,j} \frac{p(i,j)}{j^2}$

Long run emphasis (LRE) = $\frac{1}{n_r} \sum_{i,j} p(i,j) j^2$

Low gray-level run emphasis (LGRE) = $\frac{1}{n_r} \sum_{i,j} \frac{p(i,j)}{i^2}$

High gray-level run emphasis (HGRE) = $\frac{1}{n_r} \sum_{i,j} p(i,j) i^2$

Short run low gray-level emphasis (SRLGE) = $\frac{1}{n_r}\sum_{i,j}\frac{p(i,j)}{i^2 j^2}$

Short run high gray-level emphasis (SRHGE) = $\frac{1}{n_r}\sum_{i,j}\frac{p(i,j)i^2}{j^2}$

Long run low gray-level emphasis (LRLGE) = $\frac{1}{n_r}\sum_{i,j}\frac{p(i,j)j^2}{i^2}$

Long run high gray-level emphasis (LRHGE) = $\sum_{i,j} p(i,j)i^2 j^2$

Gray-level non-uniformity (GLNU) = $\frac{1}{n_r}\sum_i\left(\sum_j p(i,j)\right)^2$

Run-length non-uniformity (RLNU) = $\frac{1}{n_r}\sum_j\left(\sum_i p(i,j)\right)^2$

Run percentage (RP) = $\frac{n_r}{\sum_{i,j}(jp(i,j))}$

Where n_r corresponds to the number of homogenous runs.

4. Neighborhood gray-level different matrix (NGLDM)

NGLDM means the difference of gray levels between adjacent voxels of 8 in 2D and 26 in 3D:

Coarseness = $\frac{1}{\sum_i p(i,1)p(i,2)}$

Contrast = $\left[\sum_{i,j} p(i,1)p(j,1)(i-j)^2\right]\frac{\sum_i p(i,2)}{EG(G-1)}$

Where E is the number of voxels in VOI and G is the number of gray levels.

5. Gray-level zone length matrix (GLZLM)

GLZLM means the number of homogenous zones of the same gray-level value in 2D or 3D:

Short-zone emphasis (SZE) = $\frac{1}{n_r}\sum_{i,j}\frac{p(i,j)}{j^2}$

Long-zone emphasis (LZE) = $\frac{1}{n_r}\sum_{i,j} p(i,j)j^2$

Low gray-level zone emphasis (LGZE) = $\frac{1}{n_r}\sum_{i,j}\frac{p(i,j)}{i^2}$

High gray-level zone emphasis (HGZE) = $\frac{1}{n_r}\sum_{i,j} p(i,j)i^2$

Short-zone low gray-level emphasis (SZLGE) = $\frac{1}{n_r}\sum_{i,j} \frac{p(i,j)}{i^2 j^2}$

Short-zone high gray-level emphasis (SZHGE) = $\frac{1}{n_r}\sum_{i,j} \frac{p(i,j)i^2}{j^2}$

Long-zone low gray-level emphasis (LZLGE) = $\frac{1}{n_r}\sum_{i,j} \frac{p(i,j)j^2}{i^2}$

Long-zone high gray-level emphasis (LZHGE) = $\frac{1}{n_r}\sum_{i,j} p(i,j)i^2 j^2$

Gray-level non-uniformity for zone (GLNU) = $\frac{1}{n_r}\sum_{i}\left(\sum_{j} p(i,j)\right)^2$

Zone-length non-uniformity (ZLNU) = $\frac{1}{n_r}\sum_{j}\left(\sum_{i} p(i,j)\right)^2$

Zone percentage (ZP) = $\frac{n_r}{\sum_{i,j}(jp(i,j))}$

where n_r corresponds to the number of homogenous zones.

Appendix 2 Comparisons of texture features in the total cross-sectional area between cervical LN metastasis from CUP and cervical LN involvement of ML

	Mean	SD	Mean	SD	*p*
Histogram					
Skewness	0.091	0.206	0.044	0.129	0.352
Kurtosis	3.634	0.588	3.108	0.251	0.006*
Entropy	0.851	0.069	0.782	0.092	0.012*
Energy	0.169	0.029	0.195	0.041	0.020*
GLCM					
Homogeneity	0.490	0.044	0.510	0.052	0.168
Energy	0.031	0.012	0.042	0.019	0.025*
Contrast	4.934	1.538	4.326	2.106	0.153
Correlation	0.193	0.074	0.092	0.058	0.001*
Entropy	1.673	0.142	1.538	0.185	0.019*
Dissimilarity	1.704	0.301	1.573	0.375	0.174
GLRLM					
SRE	0.873	0.029	0.873	0.029	0.890
LRE	1.718	0.237	1.706	0.226	0.877
LGRE	0.000	0.000	0.000	0.000	–
HGRE	10874	145	10976	117	0.052
SRLGE	0.000	0.000	0.000	0.000	–
SRHGE	9493	359	9585	293	0.380
LRLGE	0.000	0.000	0.000	0.000	–
LRHGE	18666	2561	18744	2560	0.904
GLNU	1396	909	482	874	0.001*
RLNU	6077	3831	1852	3039	0.001*
RP	0.833	0.038	0.835	0.038	0.809
NGLDM					
Coarseness	0.002	0.005	0.009	0.012	0.001*
Contrast	0.032	0.012	0.051	0.021	0.002*
GLZLM					
SZE	0.686	0.019	0.635	0.083	0.048*
LZE	17722	16650	6004	13327	0.003*
LGZE	0.000	0.000	0.000	0.000	–
HGZE	10874	119	10966	117	0.037*
SZLGE	0.000	0.000	0.000	0.000	–
SZHGE	7461	183	6967	939	0.209
LZLGE	1.629	1.527	0.529	1.223	0.002*
LZHGE	192145048	181187876	66039249	146795908	0.003*
GLNU	121	69	48	74	0.001*
ZLNU	455	295	136	196	0.001*
ZP	0.112	0.038	0.126	0.045	0.352

* indicates significant differences.

Appendix 3 Correlations between texture features and tumor voxels

	p
Histogram	
Skewness	0.413
Kurtosis	0.200
Entropy	0.129
Energy	–0.116
GLCM	
Homogeneity	0.043
Energy	–0.142
Contrast	–0.083
Correlation	0.575
Entropy	0.167
Dissimilarity	–0.067
GLRLM	
SRE	–0.325
LRE	0.328
LGRE	0
HGRE	–0.434
SRLGE	0
SRHGE	–0.470
LRLGE	0
LRHGE	0.280
GLNU	0.987 *
RLNU	0.991 *
RP	–0.356
NGLDM	
Coarseness	–0.477
Contrast	–0.636
GLZLM	
SZE	0.457
LZE	0.865 *
LGZE	0
HGZE	–0.329
SZLGE	0
SZHGE	0.413
LZLGE	0.871 *
LZHGE	0.861 *
GLNU	0.981 *
ZLNU	0.947 *
ZP	–0.502

* indicates correlations of more than 0.7 between texture features and tumor volume.